Available online at www.sciencedirect.com

ScienceDirect

Ceramics International 39 (2013) 9753–9758

CERAMICS INTERNATIONAL

www.elsevier.com/locate/ceramint

Short communication

LSCM–YSZ nanocomposites for a high performance SOFC anode

Inyong Jung[a], Daehee Lee[a], Seong Oh Lee[a], Dongha Kim[a], Joosun Kim[b], Sang-Hoon Hyun[a], Jooho Moon[a,*]

[a]Department of Materials Science and Engineering, Yonsei University, 50 Yonsei-ro, Seodaemun-gu, Seoul 120-749, Republic of Korea

[b]High-Temperature Energy Materials Research Center, Korea Institute of Science and Technology, Seoul 136-791, Republic of Korea

Received 29 March 2013; accepted 6 May 2013
Available online 15 May 2013

Abstract

$La_{0.75}Sr_{0.25}Cr_{0.5}Mn_{0.5}O_{3-\delta}$ (LSCM) is a promising Ni-free anode material with reliable performance. LSCM retains excellent stability in both oxidizing and reducing environments at high operating temperatures, which makes it adoptable as solid oxide fuel cell (SOFC) anodes. However, the relatively inferior catalytic activity compared to Ni composite anodes limits the applicability in SOFC systems. Nanocomposite $La_{0.75}Sr_{0.25}Cr_{0.5}Mn_{0.5}O_{3-\delta}$–$Y_{0.16}Zr_{0.84}O_{1.92}$ (LSCM–YSZ) anodes are investigated to improve the catalytic activity by effective dispersion of LSCM nanoparticles on stable YSZ backbones. LSCM–YSZ nanocomposite powders were synthesized via a polymerizable complex method. LSM–YSZ|yttria stabilized zirconia (YSZ)|LSCM–YSZ unit cells were characterized by electrochemical impedance spectroscopy and a current interruption method. Compositional mapping analysis on the LSCM–YSZ nanocomposite anode demonstrates uniform dispersion of LSCM nanoparticles and phase connectivity between LSCM and YSZ, resulting in a lower electrode polarization resistance of 1.82 Ω cm^2 and greater peak power density of 177 mW cm^{-2} at 850 °C.

Keywords: Solid oxide fuel cells; Perovskite anode; Nanocomposite

1. Introduction

Interest in low carbon and renewable power generation has increased in recent years after the recognition that greenhouse gases are environmentally harmful. Combustion of fossil fuels, the most utilized power generation method in use today, is low efficient and causes significant environmental pollution. Solid oxide fuel cells (SOFCs) are promising electrical power generators due to their high-energy conversion efficiencies, low pollutant emissions, and fuel flexibility. They hold great promise for direct utilization of transportation fuels [1]. Ni–yttria stabilized zirconia (YSZ) cermet is the most common anode material in state-of-the-art SOFCs because of its excellent catalytic activity toward hydrogen oxidation [2]. Ni–YSZ cermet consisting of a mixture of Ni and YSZ has high electronic conductivity, reasonable ionic conductivity, and high catalytic activity for hydrogen oxidation, which are desirable properties required for an efficient anode. However, Ni–YSZ is prone to carbon deposition, coking when using hydrocarbon fuels [3], sulfur poisoning [4], and nickel agglomeration upon prolonged usage [5]. In particular, the redox stability gives rise to a collapse in the microstructure, which hinders catalytic reactions at triple phase boundaries (TPB) and degrades the cell performance [6,7]. Although coking and sulfur poisoning issues can be overcome by transition metal substitution, the redox stability problem remains for Ni–YSZ anodes.

Recently, great efforts have been paid to the development of alternative anode materials for redox stable anode, such as Cu–ceria cermet [8], $La_{0.75}Sr_{0.25}Cr_{0.5}Mn_{0.5}O_{3-\delta}$ [9], $Sr_2Mg_{1-x}MnxMoO_{6-\delta}$ [10], doped (La,Sr)(Ti)O_3 [11], and $La_{0.4}Sr_{0.6}Ti_{1-x}Mn_xO_{3-\delta}$ [12]. Relevant research has focused on perovskite-type compounds [9–14]. Tao et al. first demonstrated an efficient and fully redox-stable anode based on $(La_{0.75}Sr_{0.25})Cr_{0.5}Mn_{0.5}O_3$ (LSCM) [9]. LSCM is a p-type semiconductor with a conductivity of approximately 38 S cm^{-1} in air at 900 °C and 1.5 S cm^{-1} in 5% H_2 [15]. Due to the reasonable conductivity in both oxidizing and reducing atmospheres, LSCM can be utilized as both an anode and

*Corresponding author. Tel.: +82 2 2123 2855; fax: +82 2 312 5375.
E-mail address: jmoon@yonsei.ac.kr (J. Moon).

0272-8842/$ - see front matter © 2013 Elsevier Ltd and Techna Group S.r.l. All rights reserved.
http://dx.doi.org/10.1016/j.ceramint.2013.05.022

cathode in a symmetrical SOFC, with a peak power density of 300 mW cm^{-2} at 900 °C in wet H_2 [16]. In addition, the LCSM shows high resistance to coking when using hydrocarbon fuels, although it decomposes to form MnS, La_2O_2S and α-MnOS upon exposure to 10% H_2S [17]. Zhu et al. observed the enhancement of YSZ electrolyte-supported cell performance by impregnating the YSZ backbone anode with LSCM. The peak power density for the perovskite composite anode-based cell reached 200 mW cm^{-2} at 850 °C in wet H_2, which was much greater than the cell with a pure LSCM anode [18]. However, the impregnation approach requires iterations for suitable LSCM loading and is not amenable to the fabrication of large-size SOFCs. Furthermore, the impregnation reduces the electrode porosity and cannot guarantee thorough contact of the catalytic LSCM phase with the ionic conducting YSZ backbone phase. Segregation and/or non-uniform coating of the LSCM likely occurs and eventually leads to the insufficient formation of the TPB in the electrode, diminishing the electrode performance.

Herein, a synthesis method for nanocomposite particles is presented using a polymeric complex resin approach that has been applied for advanced cathode materials [19,20]. Well-controlled composite particles produced a better anode structure with enhanced performance in which LCSM and YSZ are intimately connected with the uniform phase distribution. Two different starting powders were used to fabricate the composite anodes: a simple micro-scale mixture of LSCM and YSZ and nanoscale composite powders. Special attention was given to the influence of the anode powder type on the cell performance via electrochemical impedance spectroscopy, a current interruption method and microstructural investigations.

2. Experimental procedure

2.1. Powder preparation

LSCM–YSZ nanocomposite powders were synthesized by a polymerizable complex resin method. The details of the synthetic procedure were described in our previous studies [19–21]. Stoichiometric amounts of nitrate salts of La, Sr, Cr, or Mn were dissolved in de-ionized water, and then ethylene glycol and citric acid were added. Polymerization between metal cation–organic complexes and ethylene occurred upon heating, resulting in a polymeric resin containing metal cations. YSZ particles (Tosoh TZ8Y, surface area=12.74 $m^2\,g^{-1}$, mean particle size=78 nm) were suspended in the polymeric resin solution. The resin mixture was then pyrolyzed in air at 400 °C for 2 h to eliminate the volatile species, followed by calcination at 1100 °C in an air atmosphere. A simple powder mixture of LSCM and YSZ was also prepared by ball milling the polymeric resin complex-derived LSCM powder and commercial YSZ powder. All the composite particles had the same overall compositions of LSCM:YSZ=75:25 wt%.

2.2. Characterization of the synthesized particles

X-ray diffraction (XRD, Rigaku D/max-Rint2100) was used to characterize the synthesized LSCM–YSZ nanocomposite powders and determine whether chemical reactions occurred when the LSCM–YSZ composite was fired at various temperatures (as-charred, 900, 1000, and 1100 °C) for 4 h. A high resolution transmission electron microscope (HRTEM, JEM-ARM200F, JEOL) operated at 200 kV was utilized to observe the morphology of the synthesized particles. Scanning transmission electron microscopy (SEM) images were taken with a 1024 × 1024 digital CCD camera, and energy dispersive X-ray (EDX) data were obtained to determine the compositional distribution.

2.3. Fabrication and characterization of electrochemical cells

An electrolyte-supported symmetric LSCM–YSZ|YSZ|LSCM–YSZ half-cell was fabricated. Electrochemical cells were prepared using two different types of LSCM–YSZ particles: synthesized nanocomposites (LYNC) and a mechanical mixture of the synthesized LSCM and YSZ (LYMM). First, commercially available YSZ powders were pressed into a pellet and sintered at 1500 °C for 5 h in air. An YSZ disk with a diameter of 20 mm and a thickness of 0.5 mm was obtained. The composite anode layers were deposited on both sides of the YSZ electrolyte by screen-printing using paste materials that were a mixture of the powders and additives dispersed in an organic solvent, α-terpineol (Sigma-Aldrich Co.), which was then fired at 1200 °C for 2 h. After sintering, a platinum mesh connected to a platinum wire was attached to the anode layer for current-collection via a platinum paste. The area of the applied anode was 1 cm^2 and the thickness was approximately 30 μm. The electrolyte-supported unit cells of LSM–YSZ|YSZ|LSCM–YSZ were also fabricated. The composite anodes were produced in the same manner as described above. A LYMM composite cathode was printed on the other side of the YSZ electrolyte and sintered at 900 °C for 4 h [19]. The areas of the applied cathode and anode were 1 cm^2 and their thicknesses were approximately 10 and 30 μm, respectively.

The electrochemical property measurements were performed for the symmetric half cells using AC impedance spectroscopy (Solartron SI 1260/1287). The impedance spectra were obtained in a frequency range of 100–0.01 Hz with applied AC voltage amplitude of 20 mV at 850 °C. Hydrogen with 4% water vapor was fed to both sides. The performance of the LSM–YSZ|YSZ|LSCM–YSZ unit cell was measured at 850 °C by the current interruption method with a potentiostat (Solartron 1287A), while feeding hydrogen to the anode and artificial air to the cathode.

3. Results and discussion

The synthesized LSCM–YSZ nanocomposite powders were analyzed by XRD to investigate the phase purity and crystalline structures. Fig. 1 shows XRD patterns of the LSCM–YSZ nanocomposite as a function of the calcination temperature. As-charred powder exhibited broad, weak peaks because it contained an unreacted amorphous LSCM phase and intact polymer complex resins. Kakihana et al. [21] revealed that the desired crystal phases were formed from the resin complex

when calcined at approximately 600 °C to decompose the polymer precursors. Calcination of the as-charred sample eliminated the amorphous phases, but the powders calcined below 1100 °C retained the impurity peaks, which corresponded to crystalline $SrCrO_4$. Only LSCM and YSZ phases without secondary and/or impurity phases appeared when calcined at 1100 °C. This result is in good agreement with a previous report by Tao et al. [15] in which LSCM–YSZ anodes were fired at 1100–1300 °C for calcination and sintering.

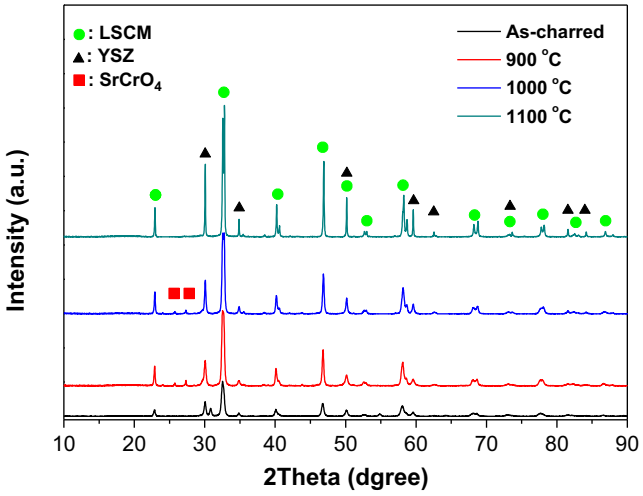

Fig. 1. X-ray diffraction patterns of the synthesized LSCM–YSZ nanocomposite powders as a function of calcination temperature.

The particle size of the LSCM calcined at 1100 °C was determined by TEM analysis. The primary particle size of LSCM was approximately 50 nm based on the TEM photograph in Fig. 2a, and the particles had a relatively uniform size distribution. Fig. 2b shows the synthesized LSCM–YSZ nanocomposite particles, and energy dispersive X-ray spectroscopy (EDX) revealed the elemental distribution of the nanocomposite particles. La, Sr, Cr, and Mn components were uniformly distributed on the LSCM particles. YSZ particles in the range of 150–200 nm are located on the left of the picture, while LSCM particles were uniformly present over the YSZ particles. EDX compositional mapping indicated that the polymeric resin method effectively produces the nanocomposite particles in which the LSCM and YSZ phases are well mixed. These nanocomposite LSCM–YSZ particles are expected to develop a better microstructure with improved phase contiguity, homogeneity, and greater TPB density than the mechanically-mixed composite particles [22].

The impedance spectra for the symmetrical cells with two different composite electrodes are shown in Fig. 3. The total interfacial polarization resistances of the LSCM–YSZ nanocomposite (denoted as LYNC) and mechanically-mixed LSCM–YSZ composite (denoted as LYMM) at 850 °C in wet H_2 were 1.82 and 2.54 Ω cm^2, respectively. The anode polarization resistance (R_p) is denoted as half of the total interfacial polarization

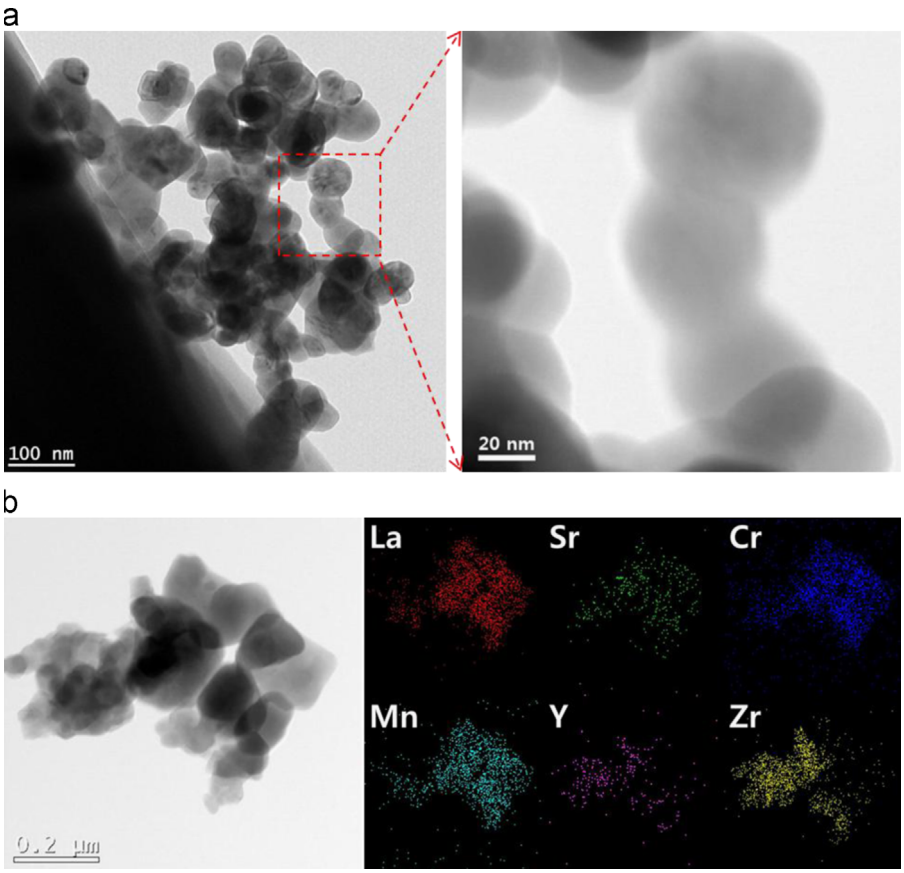

Fig. 2. (a) High-resolution transmission electron microscope (HRTEM) image of LSCM single phase powders calcined at 1100 °C, and (b) LSCM–YSZ nanocomposite powders calcined at 1100 °C and corresponding EDX elemental mapping image.

resistance of the symmetrical cell composed of two symmetrical electrodes. The high frequency intercept in the impedance spectra represents the ohmic resistance of the electrolyte and current collector, whereas the resistance from the low frequency to high frequency intercept can be treated as the polarization resistance of the anode. The R_p for the LYNC anode was less than that of the LYMM anode. The anodic polarization resistance was determined by the TPB site density and ionic/electronic conductivities. The lower R_p of the LYNC arises from the greater TPB site density and well-established ionic and electronic pathways formed through homogeneous mixing of LSCM and YSZ at nanometer length scale.

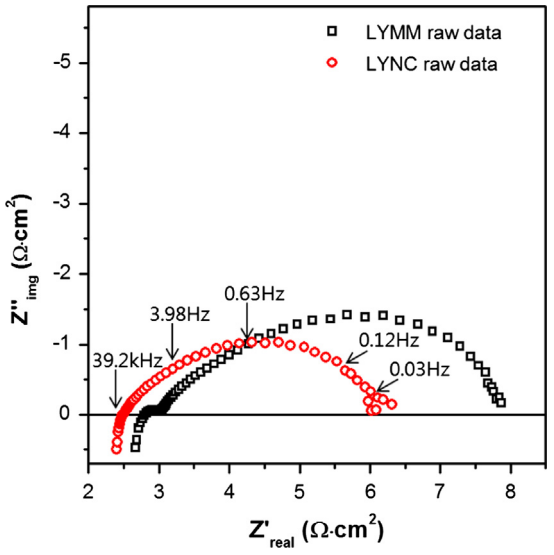

Fig. 3. Nyquist plots of the total impedance of the symmetrical LSCM–YSZ cells composed of either the mechanically-mixed LSCM–YSZ (LYMM) or nanocomposite LSCM–YSZ (LYNC) electrodes measured at 850 °C in wet H_2.

Fig. 4. Equivalent circuit model for the fitting of the LSCM–YSZ composite anodes. R_{ohmic} is the electrolyte resistance, and R_a and CPE_a, R_b and CPE_b, and R_c and CPE_c are the electrode polarization resistance and constant phase element at high frequency, medium frequency, and low frequency, respectively.

In general, the anode of SOFCs can be modeled as an equivalent parallel circuit comprised of a resistor and constant phase element (CPE), as shown in Fig. 4. The polarization resistance is further divided into high, mid, and low frequency polarization resistances, denoted as R_a, R_b, and R_c, respectively. The R_a is independent of the hydrogen partial pressure, while R_b and R_c exhibit dependence on the hydrogen partial pressure [2]. The R_a value is influenced by the transport of the charged species, i.e., oxygen ions, through YSZ [23,24], whereas R_b is influenced by the gas diffusion process through the electrode. In particular, low frequency resistance, R_c, is a strong function of the reactant concentration so that R_c is related to the catalytic conversion efficiency of hydrogen molecules to ions. [25] In order to separate the impedance arcs into R_a, R_b and R_c, the polarization resistance of the LSCM–YSZ anodes was evaluated as a function of the hydrogen partial pressure (P_{H_2}). Fig. 5a shows the impedance spectra for the LSCM–YSZ nanocomposite electrode measured at 850 °C under various H_2/N_2 mixtures (10–100% H_2) in which the interfacial polarization resistances increased with the decreasing hydrogen partial pressure. Jensen et al. suggested the use of a difference plot, in which the difference in the derivative of the impedance spectrum with respect to the frequency (f) obtained at both the specific hydrogen partial pressure and reference hydrogen partial pressure (1 atm) (i.e., $\Delta\left(\partial Z_{real}/\partial \ln f\right) = (\partial Z_{real}^{P_{H_2}=1\ \mathrm{atm}}/\partial \ln f) - (\partial Z_{real}^{P_{H_2}}/\partial \ln f))$ is plotted against $\log f$ [24]. Such a graphical representation allows the frequency determination at which the resistance variation is greatest under varying hydrogen partial pressures. Fig. 5b shows the difference plot under five hydrogen partial pressure conditions. The inflection point of the relative difference in the derivative of the resistance appeared at a frequency of 0.19 Hz, which corresponded to a summit frequency (f_{SUM}) for the R_c arc in the low-frequency region. The summit frequencies for R_a and R_b arcs in the high- and mid-frequency regions were 12.58 kHz and 5.97 Hz based on fitting with an equivalent circuit model (Fig. 4).

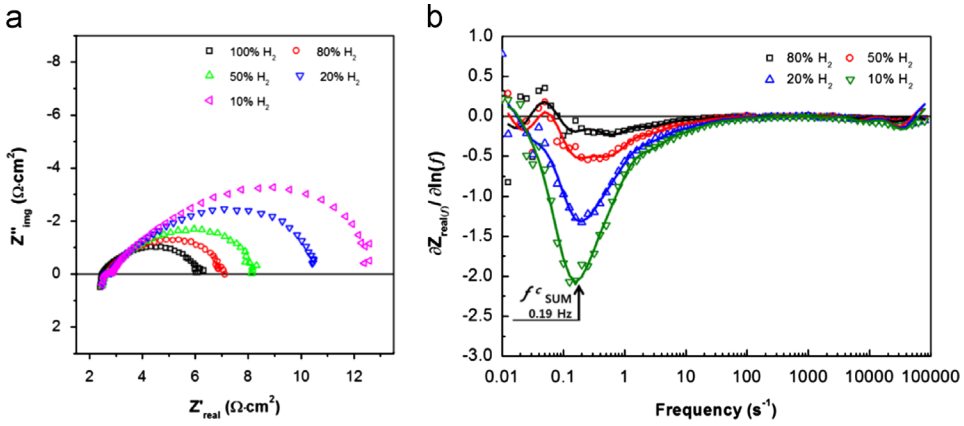

Fig. 5. (a) Nyquist plots of symmetrical cells with the nanocomposite LSCM–YSZ (LYNC) electrode measured at 850 °C as a function of hydrogen concentration (10–100% wet H_2). (b) Difference plot of $\Delta(\partial Z_{real}/\partial \ln f) = (\partial Z_{real}^{P_{H_2}=1\ \mathrm{atm}}/\partial \ln f) - (\partial Z_{real}^{P_{H_2}}/\partial \ln f)$ versus log (f) with hydrogen concentrations varying from 10 to 100% in wet H_2 at 850 °C.

The fitted spectra with equivalent circuit model well-matched the experimentally obtained spectra for the LSCM–YSZ anodes, as shown in Fig. 6. The resolved polarization resistances, R_a, R_b and R_c, are summarized in Table 1. The nanocomposite LYNC anode exhibited smaller R_a and R_b values than the mechanically-mixed LYMM anode, indicating the formation of well-connected LSCM and YSZ phases. The use of nanocomposite powders can enhance the connectivity of the electronic-conducting phase (LSCM) and ionic conducting phase (YSZ) because of better mixing of the two phases at the nanometer scale. The smaller R_a value of the nanocomposite anode, which is related to the transport of oxygen ions through the YSZ of the composite anode, implies that the well-connected YSZ phase allows for efficient conduction of oxygen ions from the electrolyte to the TPB, reducing the R_a value. The good connectivity of LSCM and YSZ of LYNC also enhances the pore structure and tortuosity so that the R_b value of LYNC is less than that of LYMM. Similar values of R_c are reasonable because the same catalyst of LSCM is used in both LYNC and LYMM.

The performances of the unit cells with two different composite anodes, LSM–YSZ|YSZ|LSCM–YSZ (nanocomposite) and LSM–YSZ|YSZ|LSCM–YSZ (mechanically mixed), are shown in Fig. 7a. The cells with LYNC and LYMM exhibited a maximum power density of 177 and 136 mW cm^{-2} at 850 °C, respectively. The total polarization resistance of the

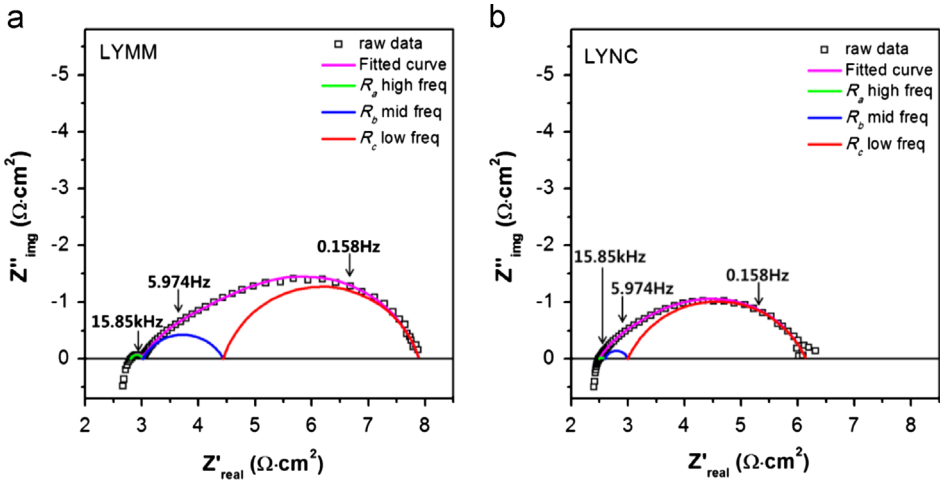

Fig. 6. Nyquist plots of the total impedance and fitted curves of the symmetrical LSCM–YSZ cells composed of either mechanically-mixed LSCM–YSZ (LYMM) or nanocomposite LSCM–YSZ (LYNC) electrodes measured at 850 °C in wet H_2. Three different curves (raw data, equivalent circuit model fitted curves, and deconvoluted curves) with summit frequencies are also shown.

Table 1
Ohmic resistance (R_{ohmic}), total interfacial polarization resistance (R_p), high frequency polarization resistance (R_a), mid frequency polarization resistance (R_b), and low frequency polarization resistance (R_c) for the LSCM–YSZ composite anodes separated by a fitting equivalent circuit model.

Composite type	R_{ohmic} (Ω cm^2)	R_p (Ω cm^2)	R_a (Ω cm^2)	R_b (Ω cm^2)	R_c (Ω cm^2)
LYMM	2.805	2.544	0.107	0.710	1.727
LYNC	2.491	1.824	0.053	0.195	1.576

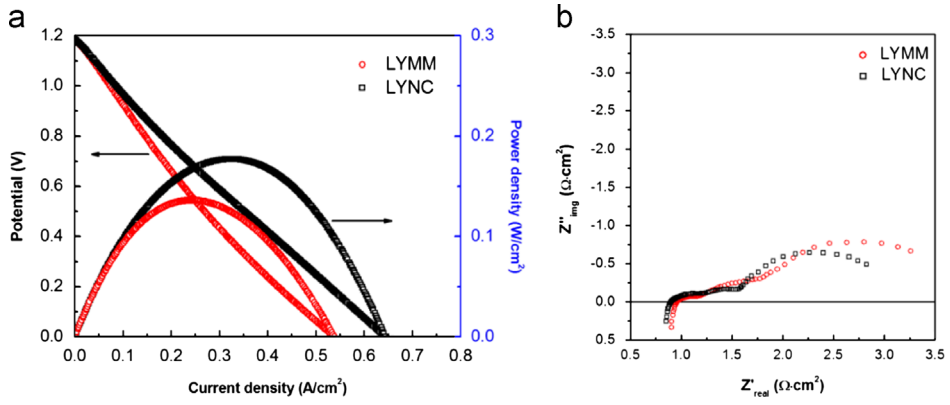

Fig. 7. (a) The unit cell performance of the LSM–YSZ (cathode)|YSZ|LSCM–YSZ with mechanically-mixed LSCM–YSZ (LYMM) and the nanocomposite LSCM–YSZ (LYNC) anodes. (b) The corresponding electrochemical impedance spectra of LSM–YSZ|YSZ|LSCM–YSZ with LYMM and LYNC anodes.

cell with LYNC was less than that of LYMM, as shown in Fig. 7b. LYMM and LYNC unit cells showed total polarization resistances of 2.57 and 2.15 $\Omega\,cm^2$ at 850 °C, respectively. This result is consistent with the impedance data for the symmetrical half cells. These observations show that the well-dispersed nanocomposite plays a key role in producing the anode microstructure in which the well-interconnected structure of LSCM and YSZ directly improved the electrochemical performance.

4. Conclusions

A LSCM–YSZ nanocomposite (LYNC) anode was fabricated for a perovskite-based redox stable anode of SOFCs, which was compared to the mechanically-mixed LSCM–YSZ anode (LYMM). The nanocomposite anode develops an ideal microstructure with improved phase contiguity and homogeneity. The electrochemical impedance spectroscopy of symmetrical half cells exhibited an improved microstructure, by which the polarization resistance caused by the transport of oxygen ions through the composite electrode and the resistance induced by the gas diffusion process were decreased by the use of LYNC. The unit cell performance of LYNC consistently exhibited better performance than that of LYMM. The LYNC produces less interfacial polarization resistance and better unit cell performance (1.82 $\Omega\,cm^2$, 177 $mW\,cm^{-2}$ at 850 °C). These results indicated that fine-tuning of the microstructures with nanocomposite powders can further enhance the polarization resistance of the anode and the unit cell performance of SOFCs.

Acknowledgments

This work was supported by a National Research Foundation of Korea (NRF) grant funded by the Korean government (MEST) (No. 2012R1A3A2026417). It was also partially supported by the Second Stage of the Brain Korea 21 Project.

References

[1] N.Q. Minh, Ceramic fuel-cells, Journal of the American Ceramic Society 76 (1993) 563–588.
[2] S.P. Jiang, X.J. Chen, S.H. Chan, J.T. Kwok, K.A. Khor, $La_{0.75}Sr_{0.25})(Cr_{0.5}Mn_{0.5})O_3$/YSZ composite anodes for methane oxidation reaction in solid oxide fuel cells, Solid State Ionics 177 (2006) 149–157.
[3] K. Nikooyeh, R. Clemmer, V. Alzate-Restrepo, J.M. Hill, Effect of hydrogen on carbon formation on Ni/YSZ composites exposed to methane, Applied Catalysis A 347 (2008) 106–111.
[4] J.F.B. Rasmussen, A. Hagen, The effect of H_2S on the performance of Ni–YSZ anodes in solid oxide fuel cells, Journal of Power Sources 191 (2009) 534–541.
[5] T. Iwata, Characterization of Ni–YSZ anode degradation for substrate-type solid oxide fuel cells, Journal of the Electrochemical Society 143 (1996) 1521–1525.
[6] M. Cassidy, G. Lindsay, K. Kendall, The reduction of nickel–zirconia cermet anodes and the effects on supported thin electrolytes, Journal of Power Sources 61 (1996) 189–192.
[7] Y. Matsuzaki, I. Yasuda, The poisoning effect of sulfur-containing impurity gas on a SOFC anode, Solid State Ionics 132 (2000) 261–269.
[8] M. Asamoto, S. Miyake, K. Sugihara, H. Yahiro, Improvement of Ni/SDC anode by alkaline earth metal oxide addition for direct methane–solid oxide fuel cells, Electrochemistry Commununications 11 (2009) 1508–1511.
[9] S.W. Tao, J.T.S. Irvine, A redox-stable efficient anode for solid-oxide fuel cells, Nature Materials 2 (2003) 320–325.
[10] D. Marrero-López, J. Peña-Martínez, J.C. Ruiz-Morales, D. Pérez-Coll, M.A.G. Aranda, P. Núñez, Synthesis, phase stability and electrical conductivity of $Sr_2MgMoO_{6-\delta}$ anode, Materials Research Bulletin 43 (2008) 2441–2450.
[11] H. Kan, H. Lee, Enhanced stability of Ni–Fe/GDC solid oxide fuel cell anodes for dry methane fuel, Catalysis Communications 12 (2010) 36–39.
[12] J.C. Ruiz-Morales, J. Canales-Vazquez, C. Savaniu, D. Marrero-Lopez, W.Z. Zhou, J.T.S. Irvine, Disruption of extended defects in solid oxide fuel cell anodes for methane oxidation, Nature 439 (2006) 568–571.
[13] O.A. Marina, N.L. Canfield, J.W. Stevenson, Thermal, electrical, and electrocatalytical properties of lanthanum-doped strontium titanate, Solid State Ionics 149 (2002) 21–28.
[14] Y.-H. Huang, R.I. Dass, Z.-L. Xing, J.B. Goodenough, Double perovskites as anode materials for solid-oxide fuel cells, Science 312 (2006) 254–257.
[15] S.W. Tao, J.T.S. Irvine, Synthesis and characterization of $(La_{0.75}Sr_{0.25})Cr_{0.5}Mn_{0.5}O_{3-\delta}$, a redox-stable, efficient perovskite anode for SOFCs, Journal of the Electrochemical Society 151 (2004) A252–A259.
[16] D.M. Bastidas, S.W. Tao, J.T.S. Irvine, A symmetrical solid oxide fuel cell demonstrating redox stable perovskite electrodes, Journal of Materials Chemistry 16 (2006) 1603–1605.
[17] S. Zha, P. Tsang, Z. Cheng, M. Liu, Electrical properties and sulfur tolerance of $La_{0.75}Sr_{0.25}Cr_{1-x}Mn_xO_3$ under anodic conditions, Journal of Solid State Chemistry 178 (2005) 1844–1850.
[18] X.B. Zhu, Z. Lü, B. Wei, K.F. Chen, M.L. Liu, X.Q. Huang, W.H. Su, Enhanced performance of solid oxide fuel cells with Ni/CeO_2 modified $La_{0.75}Sr_{0.25}Cr_{0.5}Mn_{0.5}O_{3-\delta}$ anodes, Journal of Power Sources 190 (2009) 326–330.
[19] H.S. Song, S. Lee, S.H. Hyun, J. Kim, J. Moon, Compositional influence of LSM–YSZ composite cathodes on improved performance and durability of solid oxide fuel cells, Journal of Power Sources 187 (2009) 25–31.
[20] D. Lee, I. Jung, S.O. Lee, S.H. Hyun, J.H. Jang, J. Moon, Durable high-performance $Sm_{0.5}Sr_{0.5}CoO_3$–$Sm_{0.2}Ce_{0.8}O_{1.9}$ core–shell type composite cathodes for low temperature solid oxide fuel cells, International Journal of Hydrogen Energy 36 (2011) 6875–6881.
[21] M. Kakihana, M. Arima, M. Yoshimura, N. Ikeda, Y. Sugitani, Synthesis of high surface area $LaMnO_{3+d}$ by a polymerizable complex method, Journal of Alloys and Componds 283 (1999) 102–105.
[22] S. Lee, H.S. Song, S.H. Hyun, J. Kim, J. Moon, LSCF–SDC core–shell high-performance durable composite cathode, Journal of Power Sources 195 (2010) 118–123.
[23] J.D. Kim, G.D. Kim, J.W. Moon, Y. Park, W.H. Lee, K. Kobayashi, M. Nagai, C.E. Kim, Characterization of LSM–YSZ composite electrode by ac impedance spectroscopy, Solid State Ionics. 143 (2001) 379–389.
[24] S. Primddahl, J.R. Hansen, L. Grahl-Madsen, P.H. Larsen, Sr-Doped $LaCrO_3$ anode for solid oxide fuel cells, Journal of the Electrochemical Society 148 (2001) A74–A81.
[25] N. Sakai, K. Yamaji, T. Horita, H. Yokokawa, T. Kawada, M. Dokiya, Oxygen transport properties of $La_{1-x}Ca_xCrO_{3-\delta}$ as an interconnect material of a solid oxide fuel cell, Journal of the Electrochemical Society 147 (2000) 3178–3182.